Direct observation of anisotropic exciton dispersion in the 2D semiconductor CrSBr

Yiwen Song,[1,2,*] Peiyi He,[3,4,*] Weizhe Zhang,[1] Wenyuan Ouyang,[1] Wenjing Liu,[1] Jinlong Du,[3] Zuxin Chen,[5] Jiuyu Sun,[6,†] Peng Gao,[3,4,7,‡] and Yu Ye[1,8,9,§]

[1] *State Key Laboratory for Artificial Microstructure & Mesoscopic Physics and Frontiers Science Center for Nano-Optoelectronics, School of Physics, Peking University, Beijing 100871, China*
[2] *Academy for Advanced Interdisciplinary Studies, Peking University, Beijing 100871, China*
[3] *Electron Microscopy Laboratory, School of Physics, Peking University, Beijing 100871, China*
[4] *International Center for Quantum Materials, School of Physics, Peking University, Beijing 100871, China*
[5] *School of Semiconductor Science and Technology, South China Normal University, Foshan 528225, China*
[6] *Department of Applied Physics and MIIT Key Laboratory of Semiconductor Microstructure and Quantum Sensing, Nanjing University of Science and Technology, Nanjing 210094, China*
[7] *Tsientang Institute for Advanced Study, Zhejiang 310024, China*
[8] *Liaoning Academy of Materials, Shenyang, 110167, China*
[9] *Collaborative Innovation Center of Quantum Matter, Beijing 100871, China*

We report momentum-resolved measurements of exciton dispersion in multilayer CrSBr using defocus-engineered electron energy-loss spectroscopy, supported by first-principles calculations. A pronounced in-plane anisotropy is observed, with the exciton exhibiting a linear dispersion along ΓY within $|\boldsymbol{q}| < 0.007$ Å^{-1}, while remaining nearly dispersionless along ΓX. The slope reaches 7.02 eV Å, among the largest reported in low-dimensional systems. The calculations reproduce the experimentally observed linear dispersion, confirming its intrinsic origin. We attribute the anisotropic dispersion to the long-range electron–hole exchange interaction, enhanced by strong out-of-plane confinement and governed by the directional selection rules of the transition dipole moment. Comparative measurements across the magnetic phase transition from the paramagnetic to the A-type antiferromagnetic state show that the dispersion remains essentially unchanged, indicating negligible coupling between exciton propagation and magnetic order. These results establish CrSBr as a model system for investigating anisotropic exciton dynamics in low-symmetry layered semiconductors.

Excitons, Coulomb-bound electron–hole pairs, are fundamental quasiparticles governing the optical response of semiconductors[1–3]. Their dispersion relation, describing the dependence of the exciton energy on the center-of-mass momentum, plays a central role in determining the exciton effective mass[4, 5], transport behavior[6, 7], and radiative dynamics[8–10]. More broadly, exciton dispersion encodes essential information about the intrinsic electronic structure, dimensionality[11, 12], and symmetry[13] of a material, as well as the strength of its many-body interactions.

In conventional three-dimensional semiconductors, excitons near the zero-momentum limit typically exhibit a parabolic dispersion[14–16]. In contrast, theoretical studies have predicted that reducing dimensionality to the two-dimensional (2D) limit can fundamentally alter excitonic behavior. Specifically, the long-range electron–hole exchange interaction introduces a nonanalytic dependence on momentum, which can give rise to a linear exciton dispersion in the small-momentum regime near the Brillouin zone center (Γ point)[17, 18], particularly when out-of-plane confinement enhances exchange effects. This phenomenon has been extensively discussed in the context of 2D systems such as monolayer transition metal dichalcogenides (TMDCs)[11, 17] and black phosphorus[19], where reduced screening and enhanced Coulomb interactions amplify exchange effects.

Alongside rapid progress in the synthesis and characterization of 2D materials, the experimental determination of exciton dispersion has emerged as a central challenge. Momentum-resolved electron energy-loss spectroscopy (q-EELS) provides a powerful approach for directly probing these excitations in energy–momentum space[5, 12, 20–22]. Early experimental efforts, however, were limited by insufficient energy and momentum resolution, as well as by the intrinsically narrow linear-dispersion regime in many prototypical 2D materials such as TMDCs. For instance, measurements on monolayer WSe_2 reported predominantly isotropic parabolic dispersions[21], seemingly contradicting theoretical predictions. More recently, improvements in instrumental resolution, together with the identification of materials in which the exchange-induced linear dispersion becomes experimentally accessible, have enabled the direct observation of linear exciton dispersion in systems such as the quasi-2D Mott insulator Nb_3Cl_8[12] and monolayer hBN[22]. These developments highlight the evolving capability of momentum-resolved spectroscopies to resolve excitonic dynamics in low-dimensional systems.

Despite these advances, most experimental studies to date have focused on systems with in-plane isotropy, leaving the role of intrinsic lattice anisotropy in shaping exciton dispersion largely unexplored. Layered CrSBr, a van der Waals magnetic semiconductor with pronounced

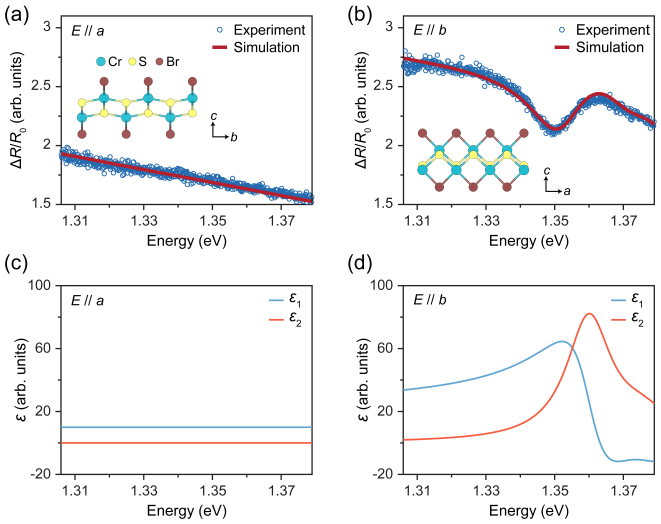

FIG. 1. Polarization-resolved optical response and extracted dielectric function of CrSBr. (a, b) Experimental differential reflectance spectra (symbols) and corresponding transfer-matrix method fits (solid lines) of a 41-nm-thick CrSBr flake at $T = 100$ K under normal incidence, with light polarized along the (a) a axis and (b) b axis. The reference reflectance R_0 was obtained from a bare silicon substrate. Inset: Crystal structure of CrSBr. (c, d) Real (ε_1) and imaginary (ε_2) parts of the calculated dielectric function along the (c) a axis and (d) b axis.

in-plane structural anisotropy[23], provides an ideal platform to address this question. Its highly anisotropic crystal structure[24] leads to strongly direction-dependent electronic[25, 26] and optical[27–29] properties. Moreover, CrSBr undergoes a magnetic phase transition from a paramagnetic state at room temperature to an A-type antiferromagnetic state below the Néel temperature ($T_N \approx 132$ K)[23, 30, 31], offering a unique opportunity to investigate the interplay between magnetic ordering and exciton dynamics within a single material system.

In this work, we employ q-EELS in a scanning transmission electron microscope (STEM), complemented by first-principles many-body perturbation calculations, to investigate exciton dispersion in free-standing multilayer CrSBr across different magnetic phases. We observe a pronounced in-plane anisotropy, characterized by a linear exciton dispersion along the ΓY direction in the small-momentum regime near the Brillouin zone center, while the ΓX direction remains nearly dispersionless. The finite-momentum Bethe–Salpeter equation (BSE) calculations faithfully reproduce the experimentally observed dispersion, confirming that it is an intrinsic property of CrSBr. Combined with an analytical model, the experiment–theory agreement identifies the linear dispersion as a consequence of long-range electron–hole exchange interaction enhanced by strong out-of-plane confinement and governed by the directional selection rules of the transition dipole moment. Furthermore, the close similarity between exciton dispersions measured in the paramagnetic and A-type antiferromagnetic phases indicates that momentum-dependent exciton dynamics are primarily determined by the intrinsic structural and electronic anisotropy, with magnetic ordering playing a negligible role. Our combined experimental and theoretical results establish the microscopic origin of the anisotropic exciton dispersion in CrSBr, providing a general framework for understanding exciton dynamics in low-symmetry layered semiconductors and for engineering directional exciton transport and anisotropy-enabled optoelectronic functionalities.

In transmission EELS, the scattering cross section is proportional to the loss function, $\mathrm{Im}[-1/\varepsilon(\omega, \boldsymbol{q})]$, where $\varepsilon(\omega, \boldsymbol{q})$ denotes the energy- and momentum-dependent dielectric function[32, 33]. A quantitative understanding of the dielectric response of CrSBr is therefore essential for interpreting its excitonic excitations. To this end, we performed polarization-resolved differential reflectance measurements on a 41-nm-thick CrSBr flake at $T = 100$ K. As shown in Fig. 1(a), the reflectance spectrum for light polarized along the a axis is nearly featureless in the energy range of 1.31–1.38 eV. In contrast, the b-axis spectrum exhibits pronounced excitonic resonances with clear absorption features [Fig. 1(b)].

To quantitatively extract the dielectric function, we fitted the reflectance spectra using the transfer matrix method (TMM)[34], modeling the complex dielectric function $\varepsilon(\omega)$ within a Lorentz oscillator formalism[35]:

$$\varepsilon(\omega) = \varepsilon_{\mathrm{bg}} + \sum_j \frac{f_j}{\omega_j^2 - \omega^2 - i\Gamma_j\omega}. \tag{1}$$

Here, $\varepsilon_{\mathrm{bg}}$ is the background dielectric constant, while ω_j, Γ_j, and f_j denote the resonance energy, linewidth, and oscillator strength of the jth excitation, respectively. For polarization along the a axis, the spectrum is well described by a constant background with $\varepsilon_{\mathrm{bg}} = 20$, indicating negligible excitonic contribution in this energy range. In contrast, the b-axis response requires two excitonic oscillators, labeled $1s$(X) and X*, centered at 1.360 eV and 1.376 eV, respectively. These resonances exhibit markedly different oscillator strengths; the X exciton dominates the optical response with $f_{\mathrm{X}} = 1.7$ (eV)^2 and $\Gamma_{\mathrm{X}} = 16$ meV, whereas the X* exciton is significantly weaker, with $f_{\mathrm{X}^*} = 0.4$ (eV)^2 and a linewidth of $\Gamma_{\mathrm{X}^*} = 20$ meV. The resulting real (ε_1) and imaginary (ε_2) parts of the dielectric function are shown in Fig. 1(c) and Fig. 1(d). Despite the inclusion of two excitonic resonances, their small energy separation (∼16 meV), comparable to their linewidths (16–20 meV), together with the strongly asymmetric oscillator strengths, renders the X* resonance a lineshape modulation rather than a distinct spectral peak.

A pronounced in-plane anisotropy of the excitonic response in CrSBr is evident, consistent with the zero-momentum optical response framework established in our

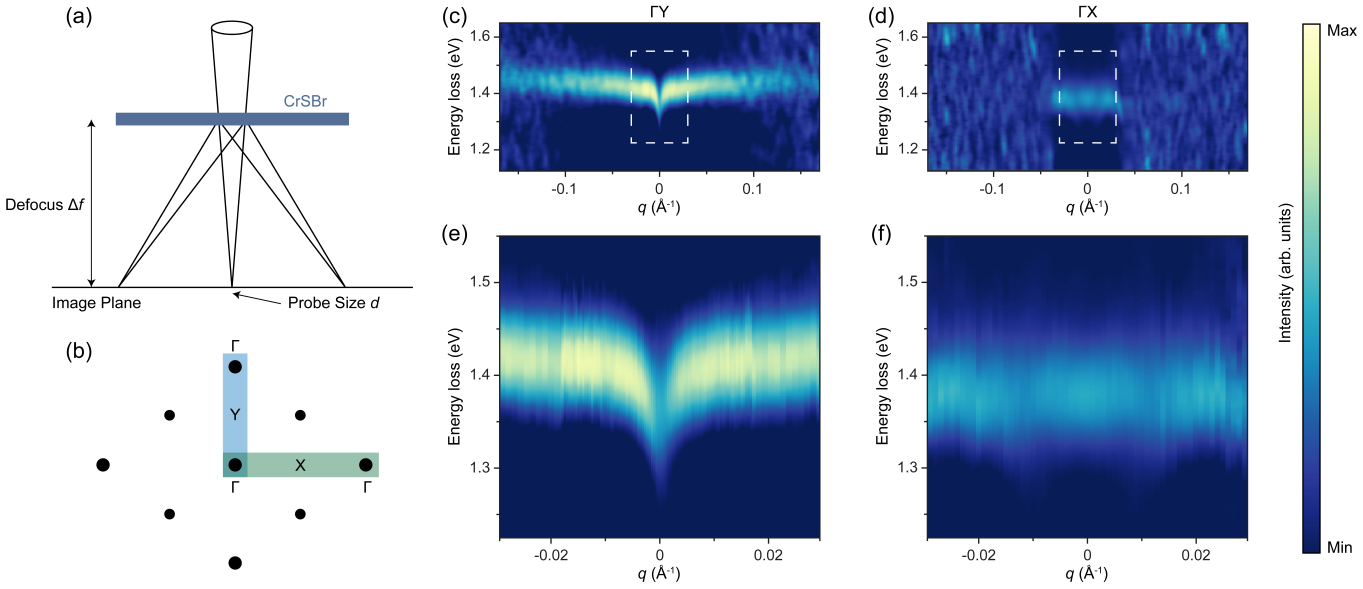

FIG. 2. Defocus-engineered q-EELS geometry and anisotropic exciton dispersion in free-standing multilayer CrSBr at $T = 100$ K. (a) Schematic illustration of the defocus-engineered q-EELS geometry. By displacing the sample from the focal plane, the electron beam becomes defocused at the sample position, causing electrons with different incident angles to spatially separate into discrete diffraction spots in the image plane. The momentum resolution (Δq) is tunable through the defocus distance (Δf). (b) Reciprocal-space geometry of CrSBr and the position of EELS slot aperture. The blue and green rectangles indicate the momentum paths along the ΓY and ΓX directions, respectively. (c, d) Normalized momentum–energy maps obtained from q-EELS measurements in multilayer CrSBr along the (c) ΓY and (d) ΓX directions, spanning a momentum range of 0.17 Å^{-1}. (e, f) Magnified views of the boxed regions in (c) and (d), respectively, covering a momentum range of 0.03 Å^{-1} near the Brillouin-zone center.

previous work[36]. The transition dipole moments are predominantly aligned along the crystalline b axis, with negligible spectral weight along the a axis. This behavior is closely linked to the in-plane anisotropic crystal structure and the quasi-one-dimensional electronic character of CrSBr[24, 26, 27]. While these zero-momentum measurements confirm the static optical anisotropy, directly probing the momentum-dependent exciton behaviors requires advanced momentum-resolved techniques.

To investigate exciton dispersion, we performed q-EELS measurements in a STEM operated at 30 kV with an energy resolution of approximately 18 meV. Multilayer CrSBr flakes (6–15 nm thick), prepared by mechanical exfoliation, were transferred onto holey carbon grids and measured at $T = 100$ K, well below the Néel temperature, corresponding to the A-type antiferromagnetic phase. To access the small-momentum regime with sufficiently high momentum resolution, we employed a defocus-engineered q-EELS geometry adapted from Midgley's approach and recently developed for low-energy dispersion measurements [37, 38]. In this configuration, the sample is displaced from the focal plane, causing the electron beam to become defocused at the sample position. As a result, electrons with different incident angles are spatially separated into discrete diffraction spots in the image plane [Fig. 2(a)]. Within the framework of Midgley theory [39], the momentum resolution Δq is related to the defocus distance (Δf) through $\Delta q = d/(\Delta f \lambda)$, where d is the probe size and λ is the electron wavelength. In the present experimental configuration, a convergence semi-angle of $\alpha = 8$ mrad together with a typical defocus value of $\Delta f = 200$ μm yields a momentum resolution of approximately 4×10^{-4} $\mathring{A}^{-1}$.

Figure 2(b) illustrates the reciprocal-space configuration of CrSBr, where the orthorhombic lattice defines two principal high-symmetry directions: ΓX (along the a axis) and ΓY (along the b axis). By adjusting the projector lens, the EELS slot aperture was aligned to selectively collect inelastically scattered electrons along these momentum directions, enabling direct mapping of exciton dispersion in momentum space.

To enhance weak signals at large momentum transfer and enable consistent comparison across different $\boldsymbol{q}$ values, the spectral intensity at each $\boldsymbol{q}$ was normalized over the energy range of 1.25–1.55 eV[40]. Momentum–energy mappings along the ΓY [Fig. 2(c)] and ΓX [Fig. 2(d)] directions exhibit mirror symmetry about the Γ point, consistent with Brillouin zone symmetry. Along the ΓY direction, excitonic features remain visible up to $|\boldsymbol{q}| \approx 0.15$ Å^{-1} and display a pronounced blueshift with increasing momentum. In the small-momentum regime near the Γ point, the exciton energy rises rapidly, forming a characteristic V-shaped dispersion. This behavior is further resolved in the magnified view of the $|\boldsymbol{q}| <$

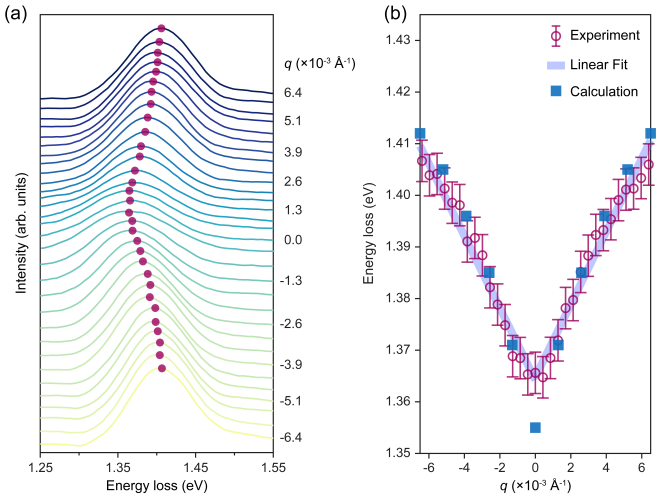

FIG. 3. Linear exciton dispersion in multilayer CrSBr near the Γ point along the ΓY direction at $T = 100$ K. (a) Momentum-resolved EELS spectra showing exciton peak evolution along ΓY. Magenta symbols denote peak positions from Gaussian fitting; corresponding momentum values (q) are on the right axis. (b) Exciton energy as a function of momentum q. Magenta circles represent the experimental peak positions extracted from q-EELS measurements, while blue squares denote the finite-momentum Bethe–Salpeter equation (BSE) calculations. The purple line is a linear fit to the experimental data, demonstrating the linear dispersion in the small-momentum regime.

0.03 Å^{-1} region [Fig. 2(e)], where the steep energy variation within the central ~ 0.01 Å^{-1} strongly indicates a nonparabolic dispersion, suggestive of a linear component in the small-momentum regime. In contrast, the dispersion along the ΓX direction exhibits markedly different behavior. Excitonic signals are only observable within a limited range of $|\boldsymbol{q}| \approx 0.04$ Å^{-1}, beyond which they become indistinguishable from the background. The corresponding magnified map [Fig. 2(f)] reveals an almost flat dispersion with negligible energy shift.

Overall, the exciton dispersion exhibits pronounced in-plane anisotropy in both the accessible momentum range and the dispersion behavior, characterized by a strong momentum-dependent blueshift along the ΓY direction, particularly in the small-momentum regime near the Γ point, suggesting a nonparabolic dispersion, in contrast to an essentially dispersionless response along the ΓX direction.

To quantitatively characterize the exciton dispersion, we extracted momentum-resolved spectra from the q-EELS mappings within a momentum range of ± 0.1 Å^{-1} around the Γ point along both the ΓX and ΓY directions. Exciton peak positions were determined by Gaussian fitting [Supplemental Material, Fig. S1], further confirming the pronounced anisotropy of the dispersion. Figure 3(a) shows representative spectra along the ΓY direction in the small-momentum regime, with magenta symbols marking the extracted peak positions. The corresponding exciton energy as a function of q is plotted in Fig. 3(b), where a linear fit (purple line) captures the dispersion near the Γ point. A clear linear dependence is observed in the small-momentum regime, followed by a gradual deviation at larger $|\boldsymbol{q}|$ [Supplemental Material, Fig. S2]. In addition to the experimental data, the finite-momentum Bethe–Salpeter equation (BSE) calculations are overlaid for comparison [computational details described in Supplemental Material]. The calculated exciton dispersion reproduces the linear energy–momentum dependence in the small-momentum regime along the ΓY direction. This excellent agreement confirms that the observed dispersion is an intrinsic property of CrSBr and provides a solid basis for understanding its microscopic origin.

The linear dispersion along the ΓY direction originates from the interplay between the orientational selection rules of the transition dipole moment and the long-range electron–hole exchange interaction. As established in Ref. [18], such exchange interaction in 2D systems introduces a nonanalytic linear term in the exciton dispersion, which for nondegenerate excitons can be generally expressed as

$$E(\boldsymbol{q}) = E_0 + A|\boldsymbol{q}|\cos^2\theta_{\boldsymbol{q}} + \frac{\hbar^2 q_x^2}{2M_x^*} + \frac{\hbar^2 q_y^2}{2M_y^*}, \qquad (2)$$

where E_0 is the exciton energy at the Γ point, A characterizes the strength of the long-range exchange interaction, $\boldsymbol{q}$ is the center-of-mass momentum, and $\theta_{\boldsymbol{q}}$ denotes the angle between $\boldsymbol{q}$ and the transition dipole moment. Here, M_x^* and M_y^* represent the effective masses of the exciton center-of-mass motion along the x and y directions, respectively.

In CrSBr, the transition dipole moment is aligned along the crystalline b axis (y direction), yielding $\cos^2\theta_{\boldsymbol{q}} = q_y^2/|\boldsymbol{q}|^2$. Substituting into Eq. (2) gives

$$E(\boldsymbol{q}) = E_0 + A\frac{q_y^2}{|\boldsymbol{q}|} + \frac{\hbar^2 q_x^2}{2M_x^*} + \frac{\hbar^2 q_y^2}{2M_y^*}. \qquad (3)$$

Along the ΓY direction ($q_x = 0$), this expression reduces to

$$E(0, q_y) = E_0 + A|q_y| + \frac{\hbar^2 q_y^2}{2M_y^*}. \qquad (4)$$

In the small-q_y limit, the linear term dominates, giving rise to the observed V-shaped dispersion. The observed linear dispersion reflects the dominance of long-range exchange interaction, enabled by strong out-of-plane confinement, rather than being a direct consequence of reduced dimensionality. Previous first-principles calculations reveal that the exciton wavefunction is strongly confined within individual CrSBr layers, with weak interlayer coupling[27]. Such out-of-plane localization enhances the

long-range exchange interaction in CrSBr, leading to the observed small-momentum linear dispersion even in this multilayer system.

Furthermore, the slope of the linear dispersion corresponds to $\hbar$ times the exciton group velocity, with $v = (1/\hbar)\, dE/dq$[41, 42], providing a direct measure of the strength of the long-range exchange interaction. The extracted slope along the ΓY direction is 7.02 eV Å, significantly exceeding that reported for monolayer MoS_2 (1.8 eV Å)[17], α-Nb_3Cl_8 (0.51 eV Å)[12], and monolayer hBN (6.08 eV Å along ΓM and 4.22 eV Å along ΓK)[22]. The unusually large exciton group velocity in CrSBr reflects an anisotropy-enhanced nonanalytic long-range exchange interaction arising from the directional alignment of transition dipole moments. Such a high group velocity establishes an intrinsic velocity scale for exciton propagation, potentially enabling efficient energy transport over mesoscopic length scales.

To further investigate the interplay between magnetic order and exciton dynamics, we performed identical q-EELS measurements on multilayer CrSBr in the paramagnetic state at $T = 300$ K [Supplemental Material, Figs. S3–S5]. A direct comparison between the paramagnetic and A-type antiferromagnetic phases reveals that the exciton dispersion is remarkably robust across the magnetic transition. In particular, the anisotropic dispersion characteristics remain essentially unchanged; the small-momentum linear dispersion along the ΓY direction persists, while the ΓX direction continues to exhibit negligible momentum dependence. Within experimental resolution, no discernible renormalization of the dispersion is observed.

A strong coupling between exciton propagation and spin degrees of freedom[36, 43] can lead to a reconstruction of the dispersion across a magnetic phase transition, manifested as momentum-dependent renormalization of the dispersion arising from exchange-driven modifications of the electronic structure and spin-dependent band splitting[44]. Such signatures are absent in our measurements. The absence of discernible changes indicates that magnetic ordering has a negligible influence on the exciton dispersion, implying a weak coupling between the exciton center-of-mass motion and the underlying spin system. Instead, the dispersion is primarily governed by the intrinsic in-plane lattice and electronic anisotropy.

In summary, we combine defocus-engineered q-EELS with first-principles calculations to resolve the momentum-dependent exciton dispersion in multilayer CrSBr. The measurements reveal a pronounced in-plane anisotropy, characterized by a linear dispersion along the ΓY direction in the small-momentum regime and a nearly dispersionless response along ΓX. The excellent agreement between experiment and theory identifies the observed anisotropic dispersion as an intrinsic property of CrSBr, originating from the long-range electron–hole exchange interaction enhanced by strong out-of-plane confinement and governed by the directional selection rules of the transition dipole moment. Despite the presence of magnetic ordering, the exciton dispersion remains essentially unchanged across the magnetic phase transition, indicating negligible coupling between exciton center-of-mass motion and the underlying spin system.

More broadly, our work establishes a general route for engineering exciton dynamics through the interplay of exchange interaction, confinement, and lattice anisotropy. This provides a framework for controlling exciton transport in low-symmetry layered semiconductors and offers new opportunities for anisotropy-driven optoelectronic functionalities.

This work was supported by the National Key R&D Program of China (Nos. 2025YFA1411002 and 2025YFA1411001), the National Natural Science Foundation of China (Nos. 12425402 and 22303041), and the Fundamental Research Funds for the Central Universities (No.30923010203). The authors acknowledge support from the High Performance Computing Platform of Nanjing University of Aeronautics and Astronautics. P.G. acknowledges the support from the New Cornerstone Science Foundation through the XPLORER PRIZE.

* These authors contributed equally to this work.
† Contact author: sunjiuyu@njust.edu.cn
‡ Contact author: pgao@pku.edu.cn
§ Contact author: ye_yu@pku.edu.cn

[1] J. Frenkel, Physical Review **37**, 17 (1931).
[2] G. H. Wannier, Physical Review **52**, 191 (1937).
[3] R. J. Elliott, Physical Review **108**, 1384 (1957).
[4] C. Habenicht, M. Knupfer, and B. Büchner, Physical Review B **91**, 245203 (2015).
[5] Z. Ahmadi Heidari and M. Knupfer, Physical Review B **111**, 205205 (2025).
[6] J. J. Crochet, J. G. Duque, J. H. Werner, B. Lounis, L. Cognet, and S. K. Doorn, Nano letters **12**, 5091 (2012).
[7] A. Ghazaryan, M. Hafezi, and P. Ghaemi, Physical Review B **97**, 245411 (2018).
[8] M. Palummo, M. Bernardi, and J. C. Grossman, Nano Letters **15**, 2794 (2015).
[9] C. Manolatou, H. Wang, W. Chan, S. Tiwari, and F. Rana, Physical Review B **93**, 155422 (2016).
[10] H.-Y. Chen, V. A. Jhalani, M. Palummo, and M. Bernardi, Physical Review B **100**, 075135 (2019).
[11] F. Wu and F. Qu, Physical Review B **91**, 075310 (2015).
[12] Z. Su, J. Mi, S. Yan, J. Li, S. Xue, Z. Tao, E. Wang, X. Shi, H. Lei, Z. Xu, J. Guo, and X. Zhu, Physical Review Letters **136**, 106502 (2026).
[13] P. Cudazzo, F. Sottile, A. Rubio, and M. Gatti, Journal of Physics: Condensed Matter **27**, 113204 (2015).
[14] M. Altarelli and N. Lipari, Physical Review B **15**, 4898 (1977).
[15] M. Gatti and F. Sottile, Physical Review B—Condensed Matter and Materials Physics **88**, 155113 (2013).
[16] R. Schuster, Y. Wan, M. Knupfer, and B. Büchner, Phys-

ical Review B **94**, 085201 (2016).
[17] D. Y. Qiu, T. Cao, and S. G. Louie, Physical review letters **115**, 176801 (2015).
[18] D. Y. Qiu, G. Cohen, D. Novichkova, and S. Refaely-Abramson, Nano letters **21**, 7644 (2021).
[19] P. Cudazzo, L. Sponza, C. Giorgetti, L. Reining, F. Sottile, and M. Gatti, Physical review letters **116**, 066803 (2016).
[20] R. Schuster, J. Trinckauf, C. Habenicht, M. Knupfer, and B. Büchner, Physical Review Letters **115**, 026404 (2015).
[21] J. Hong, R. Senga, T. Pichler, and K. Suenaga, Physical review letters **124**, 087401 (2020).
[22] L. Y. Liu, S. Y. Woo, J. Wu, B. Hou, C. Su, and D. Y. Qiu, Nature Physics , 1 (2026).
[23] E. J. Telford, A. H. Dismukes, K. Lee, M. Cheng, A. Wieteska, A. K. Bartholomew, Y.-S. Chen, X. Xu, A. N. Pasupathy, X. Zhu, C. R. Dean, and X. Roy, Advanced Materials **32**, 2003240 (2020).
[24] M. E. Ziebel, M. L. Feuer, J. Cox, X. Zhu, C. R. Dean, and X. Roy, Nano Letters **24**, 4319 (2024).
[25] F. Wu, I. Gutiérrez-Lezama, S. A. López-Paz, M. Gibertini, K. Watanabe, T. Taniguchi, F. O. von Rohr, N. Ubrig, and A. F. Morpurgo, Advanced Materials **34**, 2109759 (2022).
[26] J. Klein, B. Pingault, M. Florian, M.-C. Heißenbüttel, A. Steinhoff, Z. Song, K. Torres, F. Dirnberger, J. B. Curtis, M. Weile, A. Penn, T. Deilmann, R. Dana, R. Bushati, J. Quan, J. Luxa, Z. Sofer, A. Alú, V. M. Menon, U. Wurstbauer, M. Rohlfing, P. Narang, M. Lončar, and F. M. Ross, ACS Nano **17**, 5316 (2023).
[27] N. P. Wilson, K. Lee, J. Cenker, K. Xie, A. H. Dismukes, E. J. Telford, J. Fonseca, S. Sivakumar, C. Dean, T. Cao, X. Roy, X. Xu, and X. Zhu, Nature Materials **20**, 1657 (2021).
[28] K. Lee, A. H. Dismukes, E. J. Telford, R. A. Wiscons, J. Wang, X. Xu, C. Nuckolls, C. R. Dean, X. Roy, and X. Zhu, Nano Letters **21**, 3511 (2021).
[29] J. Sears, B. Zager, W. He, C. Occhialini, Y. Shen, M. Lajer, J. Villanova, T. Berlijn, F. Yakhou-Harris, N. Brookes, *et al.*, Physical Review Letters **135**, 146503 (2025).
[30] O. Göser, W. Paul, and H. Kahle, Journal of magnetism and magnetic materials **92**, 129 (1990).
[31] W. Liu, X. Guo, J. Schwartz, H. Xie, N. U. Dhale, S. H. Sung, A. L. N. Kondusamy, X. Wang, H. Zhao, D. Berman, R. Hovden, L. Zhao, and B. Lv, ACS Nano **16**, 15917 (2022).
[32] J. Fink, Advances in electronics and electron physics **75**, 121 (1989).
[33] K. Sturm, Zeitschrift für Naturforschung A **48**, 233 (1993).
[34] P. Yeh, *Optical Waves in Layered Media* (Wiley, New York, 1988).
[35] H. Fujiwara, *Spectroscopic Ellipsometry: Principles and Applications* (John Wiley & Sons, Chichester, 2007).
[36] T. Wang, D. Zhang, S. Yang, Z. Lin, Q. Chen, J. Yang, Q. Gong, Z. Chen, Y. Ye, and W. Liu, Nature Communications **14**, 5966 (2023).
[37] H. T. Do, M. Zhao, P. Li, Y. W. Soh, J. Rangaraj, B. Liu, T. Jiang, X. Zhang, J. Lu, P. Song, J. Teng, and M. Bosman, Nature Communications **16**, 5801 (2025).
[38] C. Elgvin, F. S. Hage, Ø. Prytz, K. Elyas, K. Höflich, C. T. Koch, and H. C. Nerl, Physical Review Materials **10**, 020201 (2026).
[39] P. Midgley, Ultramicroscopy **76**, 91 (1999).
[40] B. Liu, Y.-T. Zhang, R. Qiao, R. Shi, Y. Li, Q. Guo, J. Li, X. Li, L. Wang, J. Qi, S. Du, X. Ren, K. Liu, P. Gao, and Y.-Y. Zhang, Physical Review Letters **131**, 016201 (2023).
[41] Y. Toyozawa, Progress of Theoretical Physics Supplement **12**, 111 (1959).
[42] J. J. Thompson, S. Brem, M. Verjans, R. Schmidt, S. Michaelis de Vasconcellos, R. Bratschitsch, and E. Malic, 2D Materials **9**, 025008 (2022).
[43] M. Śmiertka, M. Rygała, K. Posmyk, P. Peksa, M. Dyksik, D. Pashov, K. Mosina, Z. Sofer, M. van Schilfgaarde, F. Dirnberger, M. Baranowski, S. Acharya, and P. Plochocka, Nature Communications (2026).
[44] A. Auerbach, *Interacting Electrons and Quantum Magnetism* (Springer, New York, 1994).